Surface Pressure Measurements on a Body Subject to Vortex Wake Interaction

A. G. Brand,* H. M. McMahon,† and N. M. Komerath‡
Georgia Institute of Technology, Atlanta, Georgia

Wind-tunnel experiments were conducted to examine the interaction effects between a rotor and an idealized airframe in forward flight. Mean and unsteady pressures were measured on the airframe suface for various flight speeds. Strong rotor-wake interactions with the airframe create large excursions in the mean pressure distribution. Extreme fluctuations in the unsteady component of pressure are also observed. The flowfield features that cause these effects are identified and discussed. It is essential that a comprehensive aerodynamic interaction code account for these features if accurate predictions of mean and unsteady airloads on the fuselage are to be obtained.

Nomenclature

b	= number of blades, (2)
c	= blade chord
Cp	= mean pressure coefficient, $(P-P_\infty)/q_\infty$
Cp'	= mean pressure coefficient, $(P-P_\infty)/(q_\infty/\mu^2)$
Cp^u	= unsteady pressure coefficient, P^u/q_∞
C_T	= thrust coefficient, $T/(\rho\pi\Omega^2R^4)$
H/R	= vertical spacing between rotor and airframe centerline
P	= mean static pressure
P^u	= unsteady component of static pressure, relative to mean
q_∞	= freestream dynamic pressure, $\rho V_\infty^2/2$
R	= rotor radius
T	= rotor thrust
V_∞	= tunnel freestream velocity
X_B/R	= axial coordinate along airframe
X_N/R	= axial position of airframe nose relative to hub
ρ	= density of air
σ	= rotor solidity, $(bc)/(\pi R)$
Φ	= angular coordinate of point on airframe
Ψ	= rotor blade azimuth angle, deg
Ω	= rotor shaft angular velocity, rad/s
μ	= advance ratio, $V_\infty/(\Omega R)$

Introduction

HELICOPTERS in forward flight are immersed in a complex flowfield. Coupled unsteady aerodynamic interactions exist between the rotor/wake and airframe that have led to problems in dynamics, performance, and handling qualities of rotorcraft. The physical features of the flowfield responsible for these problems are difficult to model analytically because the interaction mechanisms are not completely understood. This, combined with the three-dimensional unsteady nature of the rotor wake, poses a difficult challenge to designers and to those who formulate codes intended for predicting rotorcraft behavior.

A comprehensive survey by Phillipe et al.[1] discusses the current status of rotorcraft aeromechanics. Flow over isolated airframes is well understood, and panel methods that include boundary-layer effects[2] and separation[3] have been developed. Treatment of isolated rotors is at much less developed stage, especially in the forward flight regime. However, in spite of complexities in the flow and the large computational requirements, several prediction codes are available for computing the time-varying velocity field arising from a rotor and its vortical wake.[4,5]

The problem of accounting for the mutual interactions between a combined rotor and airframe in forward flight has been the subject of both analytical and experimental investigations. Johnson and Yamauchi[6] have studied the interaction problem using simplified airframe geometries. The primary emphasis of their work was in the analytical prediction of airframe effects on the rotor. Clark and Maskew[7] have approached the problem by combining a simple rotor model with a detailed airframe panel code. Recent efforts of Egolf and Lorber[8] produced encouraging results in predicting the unsteady forces generated by the rotor/wake on an airframe in forward flight.

Experimentally, Betzina and Smith[9] have carried out investigations into the steady-state mutual interaction between a rotor-body combination. Steady-state forces and moments were measured independently for both the rotor and airframe for various flight conditions. It was shown that the longitudinal aerodynamic characteristics of the airframe were significantly affected by the rotor and hub. Other experimental tests reported in Refs. 10 and 11 have measured both mean and unsteady airframe surface pressures on a rotor/airframe in forward flight. Large excursions in the mean surface pressure were observed where the edge of the rotor wake impinges on the airframe. Additionally, large amplitudes in unsteady pressure about the mean were reported.

This paper represents a continuation of the research reported in Refs. 10 and 11. It discusses some of the experimental results obtained from an investigation of the interaction phenomena associated with a rotor/airframe in forward flight. The research effort is part of a comprehensive experimental/theoretical program focusing on the interactions experienced by a helicopter in forward flight. The purpose of the experimental investigation is to gain physical insights for modeling features of the flowfield that have a significant effect on the rotor-wake/airframe interaction as well as to generate an aerodynamic interaction data base. Portions of the data base[12] have already been used for comparisons with current analytical methods.[8,10,11] It is expected that the experimental results will lead to improved prediction methods, and that the data base will ultimately provide a simple, yet complete, case for the validation of future aerodynamic interaction codes.

Facility Description

Results reported here were obtained from tests conducted in the John J. Harper 2.31 m × 2.74 m (7 × 9 ft) low-speed wind

Received May 11, 1987; revision received March 21, 1988.

*Graduate Research Fellow, School of Aerospace Engineering. Member AIAA.

†Professor, School of Aerospace Engineering. Senior Member AIAA.

‡Assistant Professor, School of Aerospace Engineering. Member AIAA.

tunnel at the Georgia Institute of Technology. The rotorcraft test configuration consists of an idealized cylindrical airframe (134 mm in diam.) with a hemispherical nose. It is supported on a sting mount, as shown in Fig. 1, independent of a two-bladed rotor that is driven by a shaft projecting down from the wind-tunnel ceiling. The airframe is fitted with static pressure taps to measure the mean surface pressure. A single row, made up of 53 taps, originates at the airframe nose and terminates at $X_B/R=2.76$. The angle Φ, locating the row around the airframe, is measured as shown in Fig. 2. Mean pressure measurements are made by digitizing and averaging analog signals from a pressure transducer over a period corresponding to 140 rotor revolutions.

Condenser microphones are used to measure the unsteady component of surface pressure, relative to the mean. Microphone ports are located in the same fashion as static pressure taps. Analog signals from microphones are digitized, and sorted into 6-deg intervals of rotor azimuth Ψ. The data within each interval are ensemble averaged over 100 rotor revolutions, and converted to Cp'' using appropriate calibration constants. The total instantaneous pressure at any microphone port is obtained by summing the mean and unsteady components.

A one-piece rotor was designed to be very stiff so that elastic motions of the blade are negligible. Blades are untwisted with constant NACA 0015 airfoil section and 86 mm chord. The 0.45 m radius R results in a solidity σ of 0.12 and a measured thrust coefficient of $C_T=0.0090$ at $\mu=0.10$. Collective and cyclic controls were eliminated in an effort to produce a compact hub with minimum aerodynamic interference. Thus, forward flight is simulated by inclining the shaft 6 deg upstream (−6 deg).

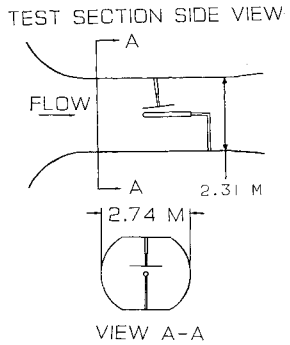

Fig. 1 Wind tunnel with rotor and airframe installed.

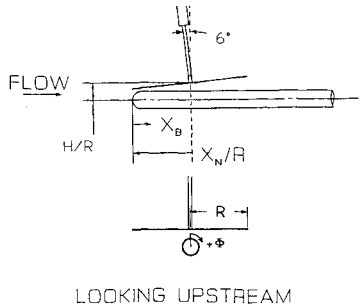

Fig. 2 Rotor and airframe geometry.

During tests, the rotor speed is kept constant at 2100 rpm, and the test section velocity is varied to achieve the desired advance ratio. Tests have been conducted for various spacing between the rotor hub and airframe centerline; however, only cases of $H/R=0.3$ are reported here. The axial distance between the rotor hub and airframe nose has also been varied, but this report concentrates only on the case where $X_N/R=-1.0$. A more thorough description of the facility and data acquisition system is given in Ref. 12. Figure 2 illustrates the notation used in this report.

The influence of wind-tunnel walls on the mean pressure measurements has been estimated using methods due to Heyson[13] and Hackett et al.[14] For advance ratios greater than 0.075, the wall interference effects on the airframe surface were found to be negligible, and no corrections were applied. No mean pressures were measured below this advance ratio. Periodic pressure amplitudes measured on the wind-tunnel floor were less than 5% of those measured on the airframe. It was thus concluded that unsteady wall effects were not significant in these tests.

Mean Surface Pressure Measurements

Airframe surface pressure distributions on helicopters in forward flight arise from both freestream and rotor/wake effects. As an aid to understanding the overall pressure distribution, it is useful to first isolate the contribution that is due to the freestream. This is considered in Fig. 3, which presents Cp along the top of the airframe in the absence of the rotor. For this test, the rotor blades were removed, but the drive shaft and hub were kept in place. As would be expected, there is flow acceleration over the hemispherical nose portion of the airframe. The hub is sensed as a local blockage to the flow, as shown by the decrease in Cp near $X_B/R=1$, where the hub is located. Later figures will indicate that this hub interference effect is substantially reduced at $\Phi=\pm45$ and is essentially zero at $\Phi=\pm90$.

The mean surface pressure distribution along the top of the airframe, with the rotor blades installed and turning, is presented in Fig. 4. The curves, which correspond to four different advance ratios, demonstrate that the rotor/wake has a profound effect on the airframe surface pressure distribution. For the three lower advance ratios, the sharp rise in pressure coefficient near $X_B/R=0.5$ indicates impingement of the leading edge of the rotor wake on the airframe surface. Flow visualization experiments were conducted, and the results (reported in Ref. 15) show that this sharp rise in Cp corresponds to the point of rotor tip vortex impingement on the airframe. Inside the wake zone, the energy added to the flow by the rotor creates a region of increased total pressure that may cause Cp to take on values greater than unity. This is especially true for low advance ratios where the freestream velocity is small compared to the velocities induced by the rotor.

In these tests, the nose of the airframe extended forward of the wake impingement zone. As a result, all advance ratios in-

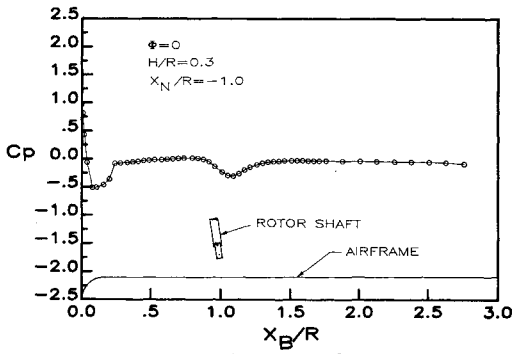

Fig. 3 Isolated airframe surface pressure.

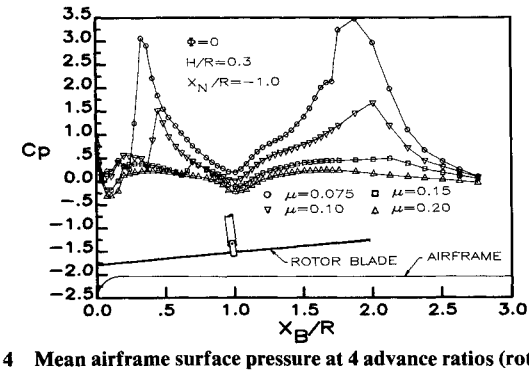

Fig. 4 Mean airframe surface pressure at 4 advance ratios (rotor on).

dicate freestream stagnation conditions at the airframe nose. Flow acceleration over the hemispherical nose is also apparent, but the presence of the rotor/wake causes each curve to deviate from the rotor-off case. Thus, the presence of the rotor affects the airframe pressure distribution both inside and in front of the wake-impingement zone.

The sweep-back angle of the wake and the spacing between the rotor and airframe (H/R) determine the location of the wake-impingement zone on the airframe. The wake sweep-back angle increases with increasing advance ratio; for constant rotor-airframe spacing, the wake-impingement zone moves rearward as advance ratio increases. At $\mu = 0.2$, the sweep-back angle is so large that Fig. 4 does not indicate any sharp impingement zone on the airframe.

A decrease in pressure coefficient near $X_B/R = 1.0$ is present for all advance ratios in Fig. 4, and it is due to the hub interference effect. Note that, since this effect is associated with the freestream and not with the rotor/wake, it does not move streamwise as advance ratio increases.

The large peak in Cp, approximately two rotor radii downstream from the nose, is caused by impingement of the rear edge of the rotor wake on the airframe. Since the rotor blades are untwisted and untapered, the rotor inflow is largest at the edges of the tip-path plane. Velocimeter measurements have verified this feature of the flow. In addition, lack of twist or taper tends to generate a strong tip vortex since blade loading is shifted outboard. These features cause the rotor-wake interaction effects to be most pronounced near the edges of the wake as shown in Fig. 4.

A general trend observed in Fig. 4 is the flattening of the curves as μ increases. This indicates that the freestream effects on the airframe become more dominant at higher forward speeds. The figure may be misleading, however, because it does not necessarily imply that the interaction with the rotor/wake diminishes with increased advance ratio. Since the measured pressure differentials $(P - P_\infty)$ are normalized by the freestream dynamic pressure q_∞, it is unclear whether the flattening trend is due to a diminished pressure differential or to the increased freestream dynamic pressure. For example, as μ approaches zero, all Cp values would approach infinty, since the measured pressure differential due to the rotor would be normalized by a very low value of q_∞.

In the absence of a rotor/wake, airframe surface pressures may be characterized as a single distribution in terms of Cp. This distribution remains unchanged in magnitude or form, regardless of freestream speed (for incompressible flow). Thus, q_∞ is appropriate for normalizing pressures when an isolated airframe is studied. In the presence of a rotor/wake, the airframe surface pressure can no longer be represented as a single characteristic distribution that is independent of freestream speed. This is a direct consequence of having two essentially separate streams (freestream and wake flow) acting on a single airframe. As a result, pressure distributions expressed in terms of Cp lead to ambiguous interpretations of the interaction strength. Thus, a new coefficient term is suggested.

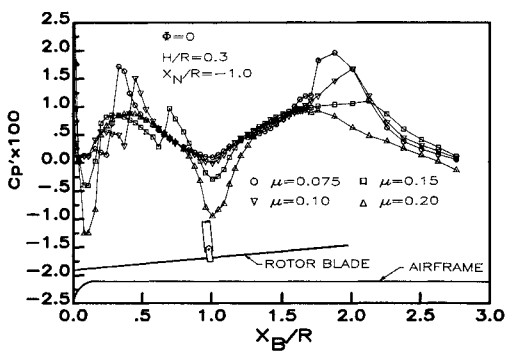

Fig. 5 Mean airframe surface pressure at 4 advance ratios, expressed in terms of modified pressure coefficient.

Normalization of pressures with the parameter q_∞/μ^2 may offer more insights for gauging the interaction strength at different flight speeds. The resulting coefficient Cp' does not become exaggerated as flight speed is decreased to $\mu = 0$. In addition, Cp' is directly related to the interaction strength (i.e., pressure differential measured on the airframe). This can be shown by writing the equivalent expression $Cp' = 2(P - P_\infty)/(\rho\Omega^2 R^2)$. The rotor tip speed ΩR is constant throughout testing. Thus, Cp' is directly proportional to the measured pressure differential regardless of μ or q_∞.

Figure 5 presents the same data as Fig. 4 except in terms of Cp'. It is seen that the pressure differentials attributed to the freestream (i.e., stagnation at the nose, acceleration over the hemispherical nose, and the hub interference) all become larger as μ increases. More importantly, Fig. 5 shows that the rotor effects do not diminish with μ as rapidly as suggested in Fig. 4. Indeed, during the course of experiments, it has been observed that the rotor effects at certain airframe locations can actually increase with μ.

In order to present a large amount of data efficiently, surface plots indicating the mean pressure distribution around the

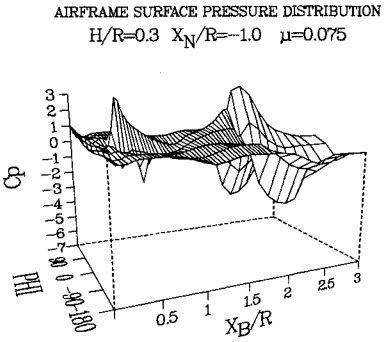

Fig. 6 Variation of mean surface pressure around airframe at low μ (PHI = Φ).

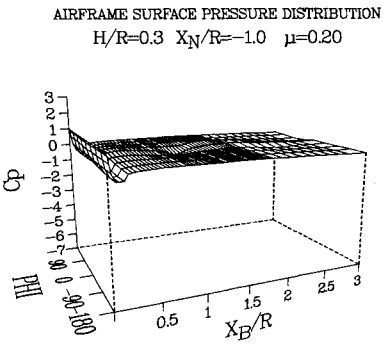

Fig. 7 Variation of mean surface pressure around airframe at high μ (PHI = Φ).

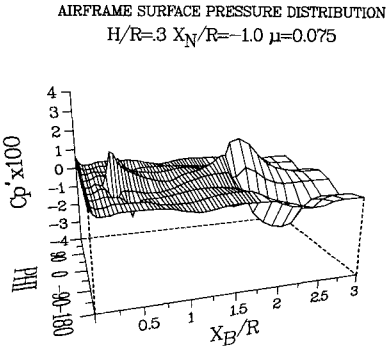

Fig. 8 Variation of mean surface pressure around airframe at low μ, expressed in terms of modified pressure coefficient.

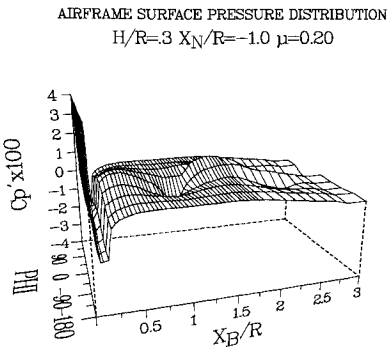

Fig. 9 Variation of mean surface pressure around airframe at high μ, expressed in terms of modified pressure coefficient.

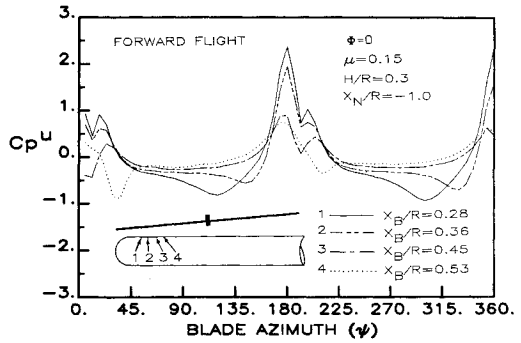

Fig. 10 Periodic surface pressure at 4 airframe locations.

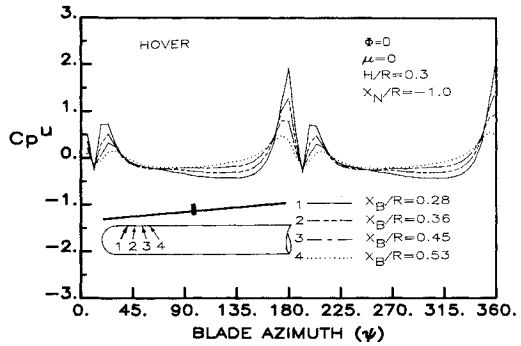

Fig. 11 Effects of blade passage on periodic pressure.

airframe have been constructed. Since the airframe is basically a circular cylinder, its pressure distribution can be projected over a flat surface by imagining the cylinder (with its measured pressure distribution) as unrolled. These results are shown in Figs. 6–9. The grid spacing is less dense over the rear third of the plots, corresponding to a wider spacing between static pressure taps on that portion of the airframe.

Figures 6 and 7 indicate surface pressure distributions, in terms of Cp, at two different advance ratios. The same data expressed in terms of Cp' are shown in Figs. 8 and 9, respectively. These figures indicate that the effect of the rotor/wake remains important at the higher advance ratio. However, the overall interaction with the airframe is strongest at the lower advance ratio of Figs. 6 and 8. At low advance ratios, the rotor/wake tends to wrap itself around the airframe as it is swept rearward. At higher advance ratios the wake, and the high energy contained in its tip vortices, is swept back so sharply that it has little opportunity to interact with the airframe.

Figure 6 indicates that the largest excursions in pressure are experienced along the top of the airframe. Based on results at a larger rotor/airframe spacing, the interaction becomes stronger as H/R is reduced. Thus, some of the largest rotor-on excursions in airframe surface pressure are expected near $\Phi = 0$, which is closest to the rotor. The large positive values of pressure occurring on the top of the airframe appear to be caused by rotor-wake flow stagnation on the surface. The lowest values of airframe surface pressure are the suction peaks observed at $\Phi = \pm 90$. These are caused by the rotor-wake flow as it accelerates around the sides of the cylindrical airframe.

Along the bottom of the airframe ($\Phi = 180$), the excursions from the rotor-off pressure distribution are minimal. At high μ, the sharply swept-back wake does not descend low enough to have a significant effect on the lower portions of the airframe. It is also possible that the airframe itself tends to shield the underside from the effects of the rotor/wake. Although flow separation is possible, tuft studies on the airframe underside revealed none at the advance ratios tested. Note, finally, that in Fig. 9 the hub interference becomes negligible at $\Phi = \pm 90$.

Periodic Surface Pressures

Condenser microphones placed at various ports in the airframe are used to measure the unsteady component of surface pressure. The output signals, expressed in terms of Cp^u, allow comparisons to be made with the mean surface pressure. The microphone data, taken as a function of the rotor azimuth angle Ψ indicate that the flow unsteadiness is periodic over one rotor revolution, and, since a two-bladed rotor was tested, the data generally repeat each 180 deg. This blade-to-blade repeatability becomes poor in certain instances when a tip vortex is very close to the measuring microphone. Possibly this is due to small differences between the blades and slight shifts in the resulting tip vortex trajectories.

At $\mu = 0.15$, the four frontmost microphone ports lie ahead of the wake impingement zone. Studying the signals from these ports allows the pressure effects of the tip vortices to be examined as they sweep back and descend toward the airframe. In Fig. 10, the periodic pressure along the top of the airframe is shown at these four consecutive ports, along with a schematic of the port locations relative to the airframe nose. It is evident that the pressure fluctuations can be quite large compared to the mean pressure excursions of earlier figures. A large contribution to flow unsteadiness occurs when the rotor blades pass above the microphones. This effect is examined in Fig. 11 for which a hovering state was achieved. In this figure, the effect of the tip vortices on the microphones is minimized, since there is no freestream to sweep them near the microphones. For purposes of comparison, the pressure disturbance due to the rotor has been normalized using the same freestream dynamic pressure that is used in Fig. 10.

A strong positive pressure peak is shown in Fig. 11, near $\Psi = 180$ deg denoting arrival of the blade leading edge over the microphone port. Since a two-bladed rotor is used, a similar signal occurs 180 deg later at $\Psi = 0 = 360$ deg. The strong positive peak is followed by a second peak of smaller magnitude, denoting passage of the blade trailing edge over the microphone port. The amount of blade rotation between passage of the leading and trailing edges depends on the chord width and the radial location of the microphone. For the microphone at $X_B/R = 0.28$, 15.2 deg of azimuthal travel are required for the entire chord to pass over the microphone. At microphone locations closer to the hub, more rotation is required, roughly 23 deg for the microphone at $X_B/R = 0.53$. The blade-passage signal is representative of the chordwise variations in the pressure field that rotates with the blade.

The hover signals in Fig. 11 are seen to be relatively flat away from the blade-passage-effect azimuth angles, indicating that the remaining wake structure (exclusive of the tip vortices) has a less significant effect on the unsteady surface pressure. The largest signal amplitudes in hover occur at the microphone labeled #1 in the figure. This is expected, since the 6-deg forward shaft tilt means that the rotor blades are closest to the microphones near the front of the airframe. Also, the aerodynamic effects of the untwisted/untapered ro-

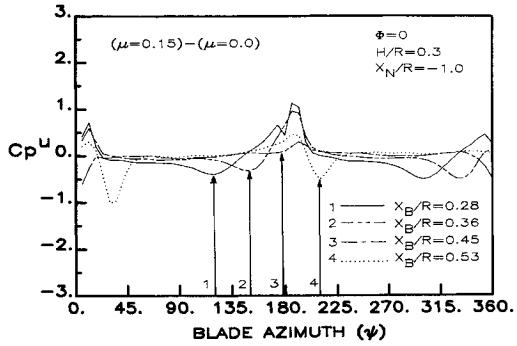

Fig. 12 Effects of tip vortex proximity on periodic pressure.

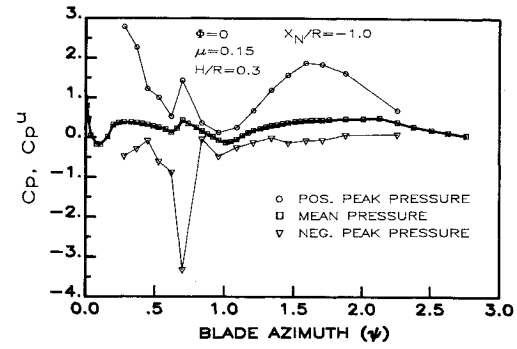

Fig. 13 Maximum peak-to-peak fluctuations in periodic pressure at low μ.

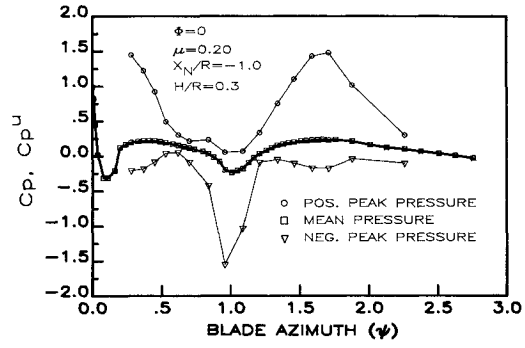

Fig. 14 Maximum peak-to-peak fluctuations in periodic pressure at high μ.

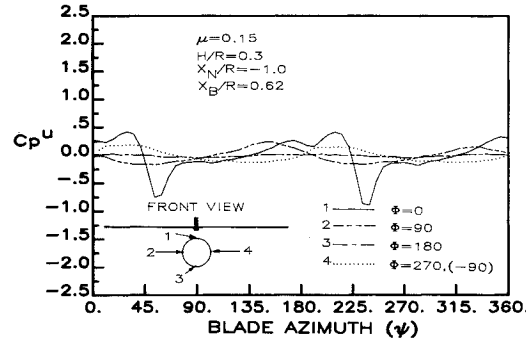

Fig. 15 Variation of periodic pressure signals around airframe.

tating blade are strongest near the tip, and weakest at the hub. Thus, the strongest signals are expected from the first microphone, and the weakest from the fourth since it is closest to the hub. Figure 10 indicates that the blade-passage pressure pulse at $\Psi = 0$ deg (or $\Psi = 180$ deg) is also present in forward flight. Thus, the significant differences between Figs. 10 and 11 are attributed to the effect of tip vortices as they convect past the microphones during forward flight.

In the previous section, Fig.4 indicated wake impingement near $X_B/R = 0.65$ at $\mu = 0.15$. This means that the tip vortices impinge on the airframe downstream of the fourth microphone. Their effect, as they pass above the microphones, is observed in Fig. 11 as a measurable dip inpressure at certain values of Ψ. In an attempt to isolate the tip vortex effect from the blade-passage pressure pulse, the hover data are subtracted from the $\mu = 0.15$ forward flight data. However, since the aerodynamic environment of the rotor in hover is greatly different from that in forward flight, this is only a crude approximation. Nevertheless, results shown in Fig. 12 give a measurable indication of the effect of tip vortex proximity on the microphone signal. In this figure, vortex proximity is indicated by the dip in Cp^u at blade azimuth angles noted with arrows. Flow visualization indicates that these dips in Cp^u correspond to the tip vortex core at its point of closest approach to the measuring microphone.

Clearly, the effect of blade passage is not completely eliminated by simple subtraction of the hover data. This presents some difficulty in analyzing signals from the third microphone because, in this case, the arrival of the blade-pressure pulse coincides with the dip in Cp^u caused by the tip vortex. This fact obscures the signature of the tip vortex at the third microphone.

Data taken at lower advance ratios reveal a much more pronounced dip in Cp^u as vortices approach the microphones and verify the observations made at $\mu = 0.15$. As the vortices move downstream and finally impinge on the airframe, a large negative peak in the unsteady surface pressure amplitude occurs. These fluctuations become more pronounced (relative to the mean) at lower advance ratios as shown by comparing Figs. 13 and 14. In these figures, the flow unsteadiness along the top of the airframe is presented for two advance ratios. The curves with circular and triangular symbols represent the peak positive and negative unsteady pressures (superimposed over the mean surface pressure), and indicate the magnitude of flow unsteadiness.

Present results indicate that the largest amplitudes in unsteady pressure coincide with the largest excursions in the mean pressure data. Previous figures showed that the mean pressure excursions were largest along the top of the airframe at ($\Phi = 0$), and much smaller underneath at $\Phi = 180$. A similar trend is observed for the amplitudes in unsteady pressure as illustrated in Fig. 15, which shows the variation in unsteady pressure signals around the airframe. For this test, four microphones were spaced at 90-deg intervals in Φ as shown. The streamwise location $X_B/R = 0.62$ and the advance ratio $\mu = 0.15$ are representative of a case in which all of the microphones lie ahead of the wake-impingement zone. At $\Phi = 0$, the effect of nearby (overhead) tip vortices is noted by a sudden dip in pressure near $\Psi = 45$ and 225 deg. Only a small signature resembling blade passage is measured at $\Psi = 0$ and 180 deg since the microphones are positioned close to the hub. The signals on the sides of the airframe ($\Phi = 90$ and $\Phi = 270$) are much smoother with lower amplitudes as well, and the effect of blade passage is not measurable. The increased vertical distance between these microphones and the rotor/wake is responsible for the reduced signature; the microphone orientation, which remains flush with the surface, may also play a role in this.

Large unsteady pressure amplitudes have been measured on the sides of the airframe at points that lie within the rotor wake. In such cases, tip vortices that drape themselves over the airframe continue to produce strong unsteady effects away from $\Phi = 0$. In Fig. 15, neither blade passage nor tip vortex effect is measurable beneath the airframe ($\Phi = 180$). However, data taken for different test conditions have shown measurable levels of unsteady pressure along $\Phi = 180$. This occurs at low advance ratios when the vortical wake structure extends below the airframe sides and persists in disrupting the flowfield.

Conclusions

Several prominent flowfield features involving rotor-wake/airframe interactions in forward flight have been identified. A strong localized pressure disturbance, proportional to q_∞, is associated with the flow around the rotor hub. Although the effect of a mast between the airframe and rotor was not examined, it appears that modeling of the rotor hub interference will be necessary for predicting airframe surface pressures accurately. This is more important when the rotor–airframe spacing is small.

The rotor/wake has a profound effect on the airframe surface pressure distribution. Energy added to the flow by rotor action accounts for large increases in total pressure inside the rotor wake. As a result, Cp may take on values in excess of unity at points on the airframe that lie within the wake impingement zone. This increased total pressure must be accounted for if accurate surface pressures, and hence, airframe forces are to be computed.

Airframe surface pressures expressed in terms of Cp' show that the overall rotor/wake interaction is reduced as μ increases. For fixed μ, the largest excursions in mean pressure occur along the top of the airframe, at the edges of the wake-impingement zone. As μ is increased, the pressure disturbances along the top of the airframe are reduced somewhat. Overall, the larger wake sweep-back angle at high μ means that a smaller portion of the airframe is exposed to wake impingement and the associated vortex interaction.

In addition to predicting the mean flow behavior, a comprehensive code must also account for the unsteady nature of the flow. The airframe exhibits pressure fluctuations at the blade-passing frequency that can be several times larger than the mean pressure excursions. These fluctuations are caused by both the rotor blades and the rotor wake. Along the top of the airframe, a pair of positive pressure pulses occur each time a blade passes overhead. This blade-passage effect is largest at portions of the airframe that lie underneath the outboard blade radii.

Vortex impingement on the airframe is also responsible for large pressure fluctuations. Along the front of the airframe, a nearby tip vortex may be detected as a local minimum in the pressure signature. Subsequent vortex impingement on the airframe results in a negative peak in pressure whose magnitude may also be several times larger than the mean pressure excursion at that point.

Acknowledgements

The authors greatefully acknowledge the support of this research effort by the U.S. Army Research Office under the Center of Excellence in Rotary Wing Aircraft Technology Program, Contract DAAG29-82-K-0094, monitored by Dr. Robert E. Singleton and Dr. Thomas Doligalski. The efforts of Mr. S.G. Liou, who assisted in conducting these experiments, are sincerely appreciated.

References

[1]Phillipe, J. J., Roesch, P., Dequin, A., and Cler, A., "A Survey of Recent Developments in Helicopter Aerodynamics," AGARD Lecture Series No. 139, Helicopter Aeromechanics, May 1985.

[2]Maskew, B., "Program VSAERO User's Guide," NASA CR-166476, 1983.

[3]Maskew, B., Dvorak, F. A., and Woodward, F. A., "Investigations of Three-Dimensional Flow Separation on Fuselage Configurations," U.S. Army Air Mobility Research and Development Lab., Moffett Field, CA, USAAMRDL-TR-77-4, March 1977.

[4]Landgrebe, A. J. and Egolf, T. A., "Prediction of Helicopter Induced Flow Velocity Using the Rotorcraft Wake Analysis," *Proceedings of the Annual Forum of the American Helicopter Society*, American Helicopter Society, Alexandria, VA, 1976.

[5]Scully, M. P., "Computation of Helicopter Rotor Wake Geometry and its Influence on Rotor Harmonic Airloads," Aeroelastic and Structures Research Lab., Dept. of Aeronautics and Astronautics, Massachusetts Inst. Technology, Cambridge, MA, Contracts N00019-73-C-0378 and N00019-74-C-0321, March 1975.

[6]Johnson, W. and Yamauchi, G. K., "Applications of an Analysis of Axisymmetric body Effects on Rotor Performance and Loads," *Proceedings of the 10th European Rotorcraft Forum*, Paper No. 3, Aug. 1984.

[7]Clark, D. R. and Maskew, B., "Calculation of Rotor/Airframe Interference for Realistic Configurations," *Proceedings of the 8th European Rotorcraft and Powered Lift Aircraft Forum*, Paper No. 2.6, Association Aeronautique et Astronautique de France, Aix-en-Provence, France, Aug. 1982

[8]Egolf, T. A. and Lorber P. F., "An Unsteady Rotor/Fuselage Interaction Method," *Proceedings for the AHS National Specialists' Meeting on Aerodynamics and Aeroacoustics,* American Helicopter Society, Alexandria, VA, Feb. 1987.

[9]Betzina, M. D. and Smith, C. A., "Rotor/Body Aerodynamic Interactions," NASA-TM-85844, Oct. 1983.

[10]Komerath, N. M., McMahon, H. M., and Hubbartt, J. E., "Aerodynamic Interactions Between a Rotor and Airframe in Forward Flight," AIAA Paper 85-1606, July 1985.

[11]McMahon, H. M. J, Komerath, N. M., and Hubbartt, J. E., "Studies of Rotor–Airframe Interactions in Forward Flight," AIAA Paper 85-5015, Oct. 1985.

[12]Brand, A. G., Komerath, N. M., and McMahon H. M., "Wind-Tunnel Data from a Rotor-wake/Airframe Interaction Study." School of Aerospace Engineering, Georgia Inst. of Technology, Atlanta, GA, Contract DAAG29-82-K-0094, July 1986.

[13]Heyson, H. H., "Jet Boundary Corrections for Lifting Rotors Centered in Rectangular Wind Tunnels," NASA TR-R-71, 1960.

[14]Hackett, J. E., Wilsden, D. J., and Lilley, D. E., "Estimation of Tunnel Blockage from Wall Pressure Signatures," NASA CR-152,241, March 1979.

[15]Brand, A. G., Komerath, N. M., and McMahon, H. M., "Results from Laser Sheet Visualization of a Periodic Rotor Wake," AIAA Paper 88-0192, Jan. 1988.